

Influences of Sn/Cu single doping and CO-doping on the structure and photocatalytic property of anatase/rutile mixed crystal TiO₂ nanomaterials under UV-visible light

Q. Qin^a, Q. Zhou^b, L. L. He^b, X. D. Zhu^{b,c,*}, W. Feng^{b,c}, J. Wang^b

^a*Intelligent Manufacturing College, Chengdu Jincheng College, Chengdu 611731, China*

^b*School of Mechanical Engineering, Chengdu University, Chengdu, 610106, China*

^c*Sichuan Province Engineering Technology Research Center of Powder Metallurgy, Chengdu, 610106, China*

Anatase/rutile mixed crystal TiO₂ nanomaterials were prepared by sol-gel method and modified by Sn/Cu single doping and co-doping. Sn doping promotes the transformation from anatase to rutile, while Cu doping inhibits the phase transformation. The inhibition effect of Cu doping on phase transition is stronger than that of Sn doping. Sn or Cu doping reduces the recombination rate, and co-doping produces a synergistic effect on the inhibition of recombination. The photocatalytic experiment results show that the photocatalytic activity of Sn-TiO₂ is higher than that of pure TiO₂ owing to higher quantum efficiency and light source absorption. The first order reaction rate constant increases from 0.00904 min⁻¹ for pure TiO₂ to 0.01476 min⁻¹ for Sn-TiO₂. Unexpectedly, the photocatalytic activities of Cu-TiO₂ and Sn/Cu-TiO₂ are lower than that of pure TiO₂. Although Cu doping improves the quantum efficiency, it reduces the absorption of ultraviolet region significantly, which is the key reason for the decline of their photocatalytic performance.

(Received October 2, 2021; Accepted January 18, 2022)

Keywords: Sol-gel method, Sn/Cu co-doping, Anatase/rutile mixed crystal, Photocatalytic performance

1. Introduction

Degradation of pollutants by TiO₂ photocatalyst materials has a broad application prospect in the field of environmental protection [1-5]. The visible light utilization and quantum efficiency of TiO₂ can be improved by modification [6-10]. Ion doping is a simple and effective way to modify the photocatalytic activity, which has been widely concerned [11-13]. Udayabhanu et al. [13] found that Cu doping improved the utilization of visible light and the separation of photogenerated electron-hole pair, promoting the photocatalytic activity. The co-doping modification may produce a synergistic effect and achieve higher photocatalytic activity than that of single element modification [14-16]. Georgieva et al. [16] prepared B and N co-doped TiO₂ nanotubes. The synergistic effect of B and N co-doping resulted in the maximum quantum efficiency, thus co-doped TiO₂ showed the best photocatalytic activity.

Anatase/rutile mixed TiO₂ exhibits higher photocatalytic efficiency than single crystal TiO₂ due to the mixed crystal effect reported by numerous researchers [17-20]. Abdullah et al. [17] found that anatase/rutile mixed crystal TiO₂ calcined at 800 °C showed higher visible light absorption and photogenerated pair separation efficiency than anatase calcined at 500 °C, exhibiting higher photocatalytic activity.

In the present work, anatase/rutile mixed crystal TiO₂ was prepared, and the effects of Sn/Cu single doping and co-doping on the structure and photocatalytic performance of mixed crystal TiO₂ were investigated in detail.

*Corresponding author: xiaodangjia21@126.com

<https://doi.org/10.15251/DJNB.2022.171.65>

2. Experimental part

2.1. Sample preparation

Solution A was obtained by adding anhydrous ethanol and tetrabutyl titanate in beaker with a volume ratio of 3:2. Deionized water, glacial acetic acid and anhydrous ethanol were mixed with a volume ratio of 4:4:15 to gain solution B, which was dropped into solution A to form a gel. After drying, it was heat treated at 550 °C for 1 h to obtain pure TiO₂, which is labeled as PT. Adding a certain amount of Cu(NO₃)₂·3H₂O or SnCl₄·5H₂O into solution B, keeping the molar ratios of Ti/Sn and Ti/Cu are 1:0.05 and the rest steps are unchanged to prepare 5%Sn-doped TiO₂ and 5%Cu-doped TiO₂, which are labeled as ST and CT, respectively. Meanwhile, Sn/Cu co-doped TiO₂ with a molar ratio of Ti/Sn/Cu=1:0.025:0.025 marked as SCT can be obtained by adding moderate Cu(NO₃)₂·3H₂O and SnCl₄·5H₂O simultaneously.

2.2. Sample characterization

A DX-2700 X-ray diffractometer was used to analyze the crystal structure (XRD). A FEI-Inspect F50 scanning electron microscope and a FEI-Tecnai G2 F20 transmission electron microscope were used to observe the morphology (SEM and TEM). An XSAM800 multifunctional surface analysis system was used to analyze the element composition and valence state (XPS). A F-4600 fluorescence spectrometer was used to analyze the photoinduced electron-hole recombination rate (PL). A UV-3600 ultraviolet-visible photometer was used to test the optical absorption (DRS).

2.3. Photocatalytic experiment

The photocatalytic performance of samples was investigated by the degradation rate of Rhodamine B solution (RhB). 200 mL RhB solution with a concentration of 10 mg/L and 0.1 g sample powder were mixed. After stirred for 30 min in dark, the mixture was irradiated by a 250 W xenon lamp. The samples were taken every 20 min to measure its absorbance at 553 nm. RhB degradation rate was calculated by the formula $(A_0 - A_t)/A_0 \times 100\%$, where A_0 and A_t are the initial and t time absorbance.

3. Results and discussion

3.1. Crystal structure

Fig. 1 shows the XRD patterns of samples. The diffraction peaks of PT at 25.3°, 37.1°, 37.9°, 38.6°, 48.2°, 54.0° and 55.2° correspond to (101), (103), (004), (112), (200), (105) and (211) crystal planes of anatase structure. The diffraction peaks at 27.3°, 36.2°, 39.4°, 41.3°, 44.2°, 54.4° and 56.7° correspond to (110), (101), (200), (111), (210), (211) and (220) crystal planes of rutile structure. PT is a mixed crystal structure composed of anatase and rutile, and the content of anatase is 69.3% and rutile is 30.7%. The rutile diffraction peaks intensity of ST is higher than that of PT, and the rutile content of ST is 85.6%, indicating that Sn doping facilitates the transformation from anatase to rutile phase. Since Sn⁴⁺ radius (0.069 nm) is slightly larger than Ti⁴⁺ radius (0.0605 nm), Sn⁴⁺ ions enter into TiO₂ lattice and replace Ti⁴⁺ ions, forming lattice defects and introducing oxygen vacancies, making Ti-O bond more prone to fracture and promoting the phase transformation [21, 22]. The CT pattern is full of anatase diffraction peaks, and there is no rutile related diffraction peak, which suggests that Cu doping inhibits the phase transformation from anatase to rutile. Cu element may be dispersed on the surface of TiO₂ in the form of oxide, which obstructs the migration of Ti and O atoms at the interface thus retards the nucleation and growth of rutile [23]. SCT is a mixed crystal structure, and the content of rutile is 7.0%, which is lower than that of PT (30.7%), indicating that the inhibition of Cu doping is stronger than the promotion of Sn doping, thus Sn/Cu co-doping inhibits the phase transformation.

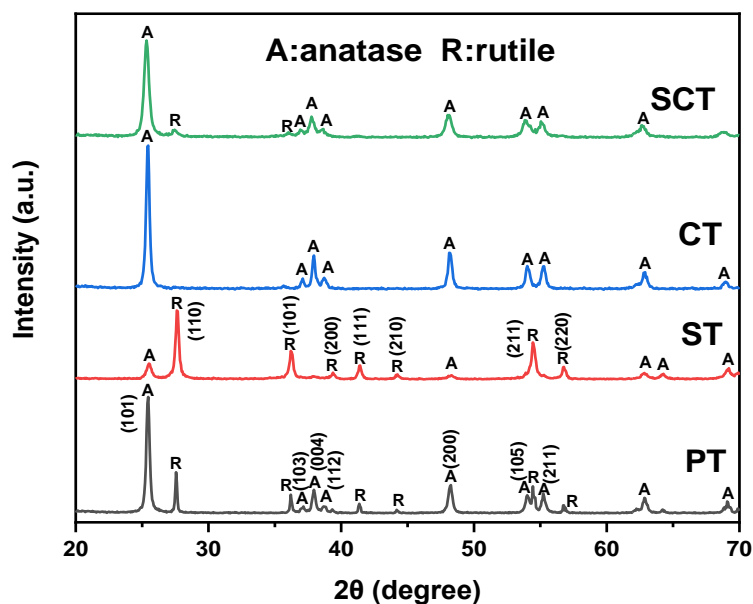


Fig. 1. XRD patterns of samples.

The average grain size of samples were calculated using Scherrer formula [24] and the results are shown in Fig. 2. The grain sizes of doped TiO_2 are less than pure TiO_2 , implying that both single doping and co-doping can refine the grains.

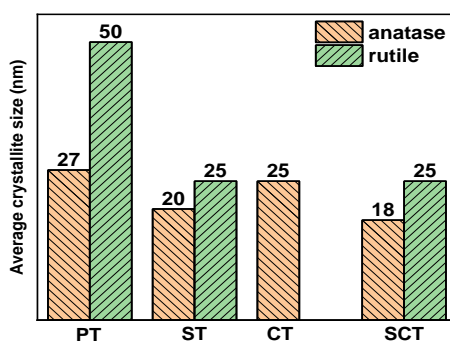


Fig. 2. The average grain sizes of samples.

3.2 Morphology

Fig. 3 presents the SEM images of samples. In Fig. 3a, it is observed that the particle morphology of PT is granular with a certain degree of agglomeration, and the agglomerate sizes are ranged from tens to hundreds of nanometers. There is no obvious difference in the morphology of doped samples, and all of them are composed of granular particles and agglomerations.

Fig. 4 shows the TEM and HRTEM images of PT (a, c) and SCT (b, d). The single particle size of PT is about 20-30 nm in Fig. 4a. In Fig. 4c, the crystal plane spacing 0.346 nm can be ascribed to the anatase (101) crystal plane and the crystal plane spacing 0.249 nm corresponds to the rutile (101) crystal plane [8], which indicates that PT forms anatase and rutile mixed crystal structure. It is observed in Fig. 4b that the single particle size is about 20-30 nm, and the interplanar spacing 0.358 nm corresponds to the anatase (101) crystal plane.

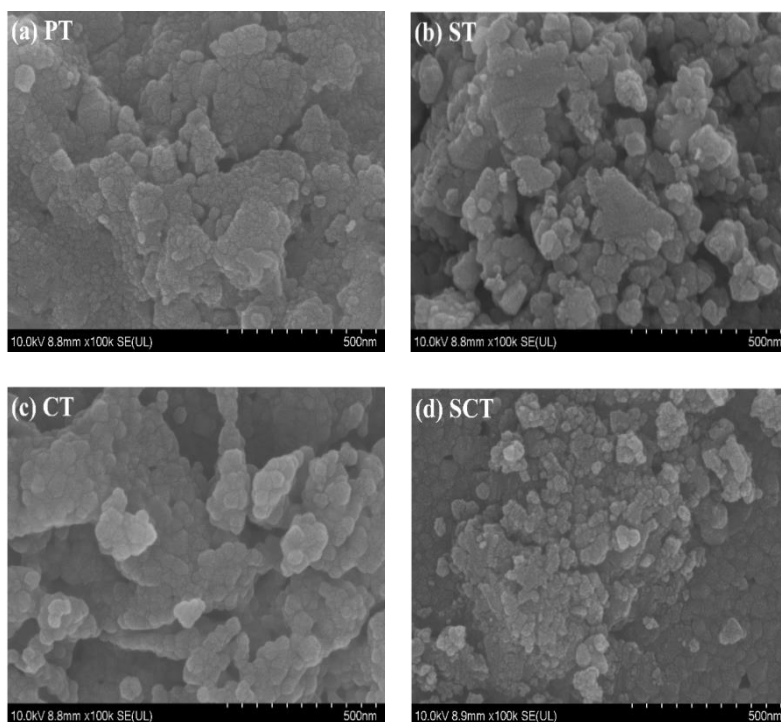


Fig. 3. SEM images of samples: (a) PT; (b) SY; (c) CT; (d) SCT.

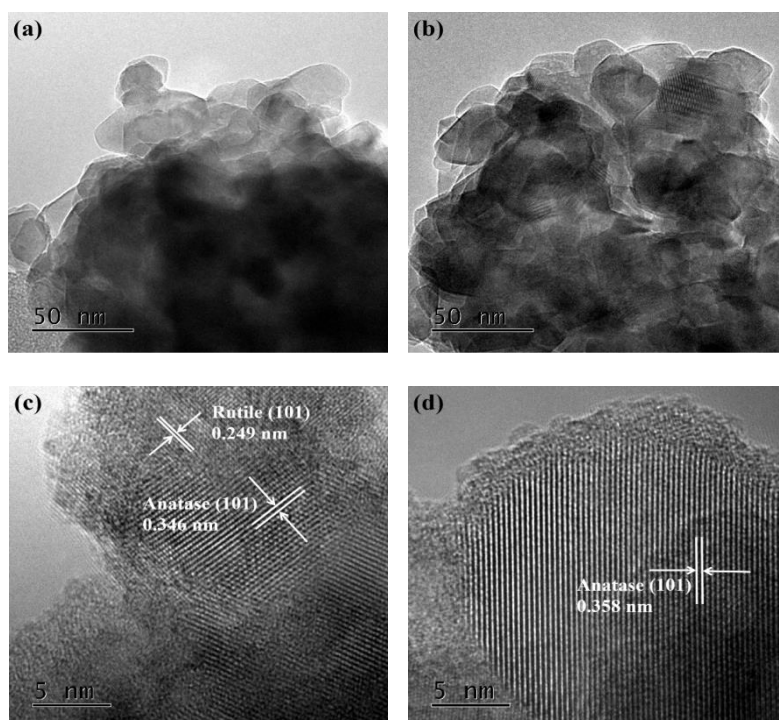


Fig. 4. TEM and HRTEM images of PT (a, c) and SCT (b, d).

3.3. Element composition and state

Fig. 5 shows the XPS spectrum of SCT. The characteristic peaks of C 1s, Ti 2p, Sn 3d, Cu 2p and O 1s appear in the full spectrum (Fig. 5a), indicating the presence of C, Ti, Sn, Cu and O

elements in the sample. The high-resolution spectrum of Ti 2p is shown in Fig. 5b. Ti 2p consists of four peaks located at 463.4 eV, 457.9 eV and 464.7 eV, 459.0 eV corresponds to $\text{Ti}^{3+} 2p_{1/2}$, $\text{Ti}^{3+} 2p_{3/2}$ and $\text{Ti}^{4+} 2p_{1/2}$, $\text{Ti}^{4+} 2p_{3/2}$, indicating that Ti element exists +3 and +4 valences [25, 26]. Fig. 4c shows the high-resolution spectrum of Sn 3d. The characteristic peaks of $\text{Sn}^{4+} 3d_{5/2}$ and $\text{Sn}^{4+} 3d_{3/2}$ appear at 486.0 eV and 494.7 eV, respectively, indicating that Sn exists as Sn^{4+} [27]. It can be seen from Fig. 5d that Cu 2p consists of four peaks located at 933.0 eV, 942.3eV, 952.9 eV and 962.3eV, suggesting that Cu element exists as Cu^{2+} and Cu^+ [12, 28, 29]. The characteristic peaks in Fig. 5e are located at 529.5 eV and 530.9 eV, corresponding to the lattice oxygen (O^{2-}) and surface hydroxyl (OH^-) [30], respectively.

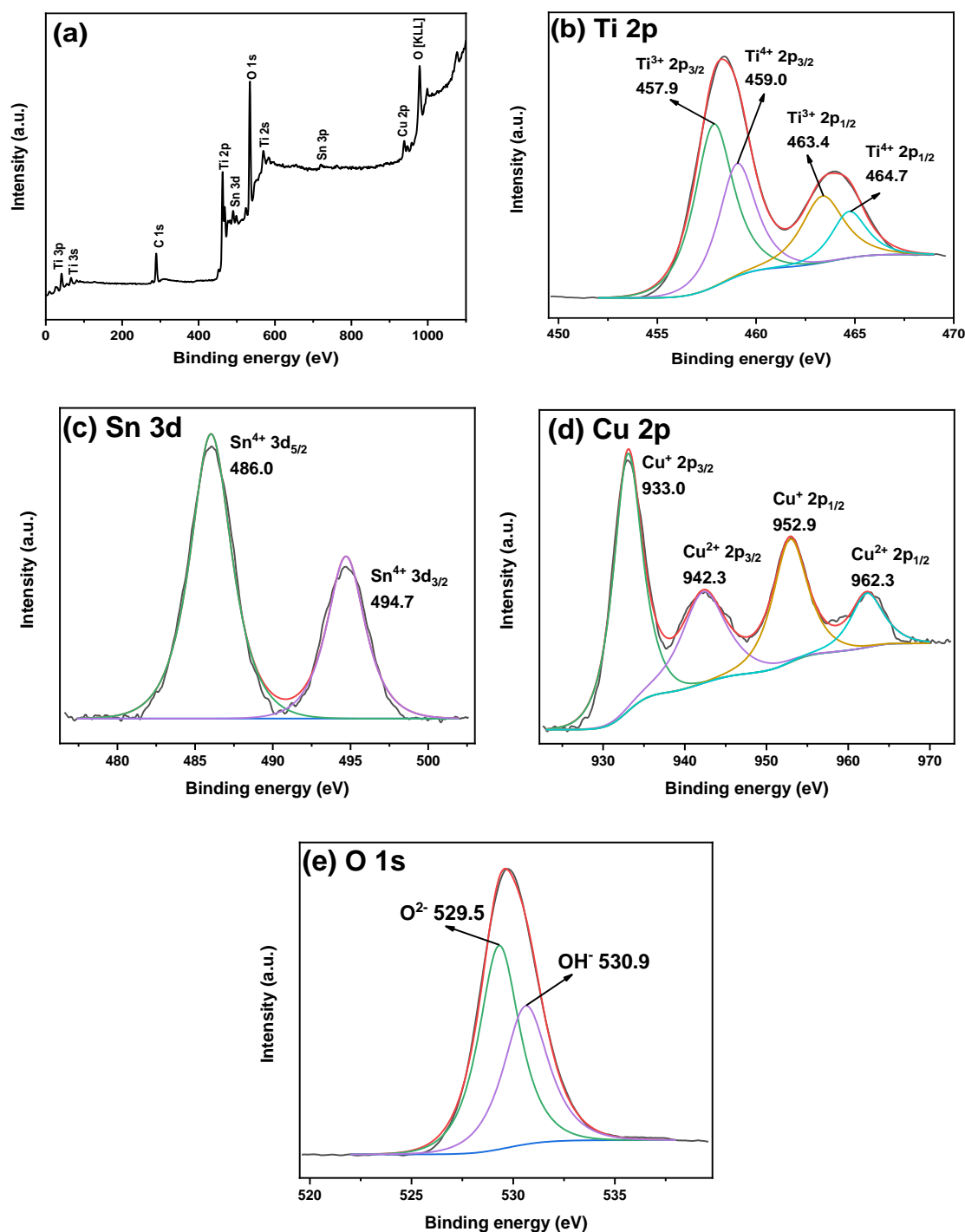


Fig. 5. XPS spectrum of SCT: (a) total spectrum; (b) Ti 2p; (c) Sn 3d; (d) Cu 2p; (e) O 1s.

3.4. Optical property

The photons will be released when photogenerated electrons and holes recombine, which is related to the PL peak intensity. Therefore, the lower PL peak intensity, the lower the recombination rate of photogenerated electrons and holes [31]. Fig. 6 presents the PL spectra of samples. The PL peak intensity of ST is lower than that of PT, indicating that Sn doping inhibits the recombination. The replacement of Ti^{4+} by Sn^{4+} introduces lattice defects and O vacancies, which capture the photogenerated charges and reduce the recombination [32]. Remarkably, the PL peak intensity decreases significantly after Cu doping. Cu oxides may be dispersed on the surface of TiO_2 , forming TiO_2/CuO and TiO_2/Cu_2O semiconductor composites. Since the conduction band of TiO_2 is higher than that of Cu oxides, the photogenerated electrons will migrate from TiO_2 conduction band to Cu oxides conduction band after being excited by light, thus reducing the recombination rate of photogenerated electrons and holes in TiO_2 [33]. SCT shows the lowest PL peak intensity, indicating that Sn and Cu co-doping produces a synergistic effect on inhibiting recombination thus exhibits the highest quantum efficiency.

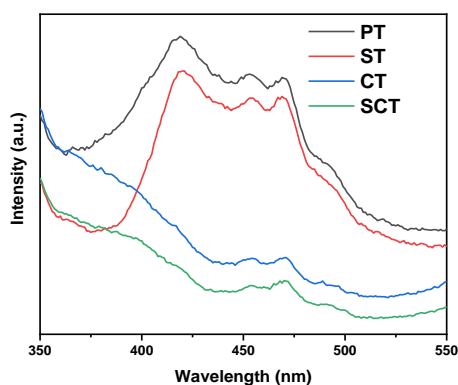


Fig. 6. Photoluminescence (PL) spectra of samples.

The UV-vis absorption spectra of samples are depicted in Fig. 7. The absorption of ST in UV region is higher than that of PT. Meanwhile, the absorption edge of ST shows a red shift compared with PT, indicating that Sn doping enhances the utilization of light source. The most noteworthy thing is that the absorption in UV region of CT and SCT decreases sharply compared to PT, which may be due to the fact that Cu oxides disperses on TiO_2 surface, preventing the absorption of light source [34]. Marked reduction of light source absorption by Cu doping is detrimental to the photocatalytic performance.

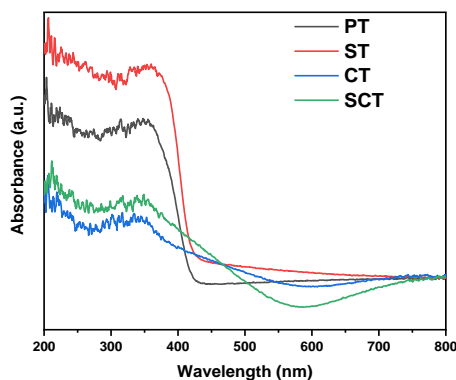


Fig. 7. Ultraviolet-visible absorption spectra of samples.

3.5. Photocatalytic activity

The photocatalytic performance of samples was evaluated by the degradation degree of RhB and the results are shown in Fig. 8. The degradation degree of ST is 78.5% after 100 min, which is higher than that of PT (58.9%), indicating that Sn doping improves the photocatalytic performance of TiO₂. The degradation degree of CT is 8.4%, which is significantly lower than that of PT, indicating that Cu doping suppresses the photocatalytic performance. The degradation degree of SCT is 11.1%, showing that the photocatalytic activity is still reduced after co-doping. The first-order reaction rate constants of PT, ST, CT and SCT are 0.00904 min⁻¹, 0.01476 min⁻¹, 0.00089 min⁻¹ and 0.00120 min⁻¹, respectively. ST exhibits the fastest reaction rate and the reaction rate of CT and SCT are less than PT, which is consistent with the results of degradation degree.

It can be concluded from optical measurement results that Sn doping is advantageous to enhancing the light utilization and quantum efficiency, thereby improving the photocatalytic performance. On the other hand, although Cu doping is beneficial to reducing the recombination of photo-generated electrons and holes, it does not elevate the photocatalytic activity. The absorption of ultraviolet light is drastically reduced after Cu doping, which may be caused by Cu oxides dispersing on the surface of TiO₂, preventing the light absorption. This is the critical reason for the decline of photocatalytic performance after Cu doping. The UV absorption of SCT is slightly higher than that of CT, as a result, the photocatalytic activity of co-doping TiO₂ is higher than that of Cu-doped TiO₂.

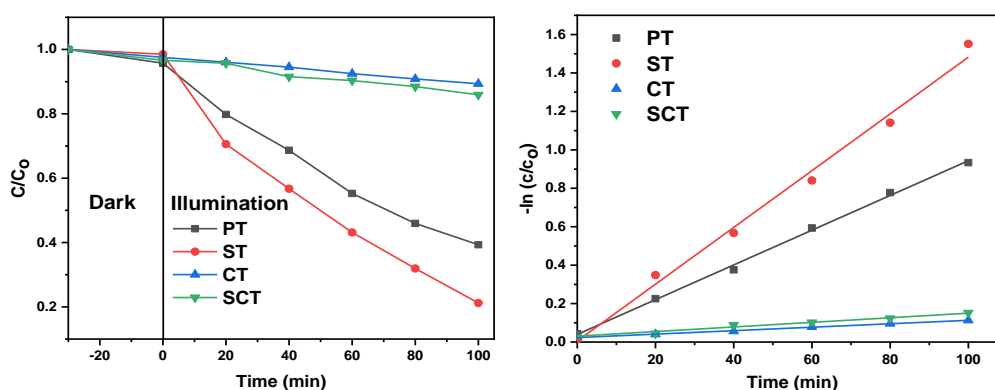


Fig. 8. Photodegradation curves (a) and kinetics fitting curves (b) of samples.

4. Conclusions

Pure and Sn/Cu doped TiO₂ were prepared by sol-gel route and characterized by XRD, SEM, TEM, XPS, PL and DRS. The results show that Sn doping promotes the phase transformation, while Cu doping inhibits the phase transformation. The inhibitory effect of Cu doping is stronger than the promotion of Sn doping, and co-doping still shows the inhibitory effect. Both Sn/Cu single doping and co-doping reduce the recombination rate of photo-generated electron-hole pairs. The absorption of light source is increased by Sn doping, however, the absorption of CT and SCT in UV region drop sharply. The photocatalytic experiment results show that Sn doping improves the photocatalytic performance of TiO₂. On the other hand, Cu doping and Sn/Cu co-doping suppress the photocatalytic performance of TiO₂ due to their poor absorption in UV region.

Acknowledgements

This work was supported by the Training Program for Innovation of Chengdu University (S202011079053, CDU-CX-2021527).

References

- [1] S. S. Arbuji et al., Materials Science and Engineering B 168, 90 (2010); <https://doi.org/10.1016/j.mseb.2009.11.010>
- [2] Y. Sun et al., Digest Journal of Nanomaterials and Biostructures 16(1), 239 (2021);

- [3] R. Cherrak et al., *Silicon* 12(4), 927 (2020); <https://doi.org/10.1007/s12633-019-00186-6>
- [4] X. T. Gao et al., *RSC Advances* 10, 40619 (2020); <https://doi.org/10.1039/D0RA08116G>
- [5] Y. Sun et al., *Digest Journal of Nanomaterials and Biostructures* 14(2), 463 (2019).
- [6] J. Singh et al., *Journal of Materials Science: Materials in Electronics* 30, 16478 (2019); <https://doi.org/10.1007/s10854-019-02023-3>
- [7] Y. Sun et al., *Materials Research Express* 7, 085010 (2020); <https://doi.org/10.1088/2053-1591/abaea4>
- [8] F. H. Wang et al., *Ceramics International* 47, 7632 (2021); <https://doi.org/10.1016/j.ceramint.2020.11.104>
- [9] X. D. Zhu et al., *Journal of Materials Science: Materials in Electronics* 30, 21210 (2019); <https://doi.org/10.1007/s10854-019-02494-4>
- [10] J. Li et al., *Ceramics International* 47, 8218 (2021); <https://doi.org/10.1016/j.ceramint.2020.11.181>
- [11] T. M. Triantis et al., *Journal of Hazardous Materials* 211-212, 196 (2012); <https://doi.org/10.1016/j.jhazmat.2011.11.042>
- [12] Udayabhanu et al., *International Journal of Hydrogen Energy* 45, 7813 (2020); <https://doi.org/10.1016/j.ijhydene.2019.10.081>
- [13] Z. H. Fan et al., *J Mater Sci: Mater Electron* 27, 11866 (2016); <https://doi.org/10.1007/s10854-016-5329-0>
- [14] M. Shaban et al., *Journal of Colloid and Interface Science* 555, 31 (2019); <https://doi.org/10.1016/j.jcis.2019.07.070>
- [15] X. D. Zhu et al., *Scientific Reports* 8, 12387 (2018).
- [16] J. Georgieva et al., *Applied Surface Science* 413, 284 (2017); <https://doi.org/10.1016/j.apsusc.2017.04.055>
- [17] L. Chetia et al., *Journal of Photochemistry and Photobiology A: Chemistry* 338, 134 (2017); <https://doi.org/10.1016/j.jphotochem.2017.01.035>
- [18] A. Z. Abdullah et al., *Journal of Hazardous Materials* 173, 159 (2010); <https://doi.org/10.1016/j.jhazmat.2009.08.060>
- [19] Q. Wang et al., *Solid State Sciences* 77, 14 (2018); <https://doi.org/10.1016/j.solidstatesciences.2018.01.003>
- [20] V. Likodimos et al., *Applied Catalysis B: Environmental* 192, 242 (2016); <https://doi.org/10.1016/j.apcatb.2016.03.068>
- [21] A. K. Alves et al., *Catalysis Today* 208, 7 (2013); <https://doi.org/10.1016/j.cattod.2012.10.020>
- [22] J. M. Dua et al., *Materials Letters* 93, 419(2013); <https://doi.org/10.1016/j.matlet.2012.11.134>
- [23] V. Krishnakumar et al., *Journal of Materials Science: Materials in Electronics* 27, 7438 (2016); <https://doi.org/10.1007/s10854-016-4720-1>
- [24] V. Uvarov et al., *Materials Characterization* 58(10), 883 (2007); <https://doi.org/10.1016/j.matchar.2006.09.002>
- [25] H. Y. Liu et al., *Applied Sciences* 1, 487 (2019).
- [26] N. R. Khalid et al., *Ceramics International* 39, 7107 (2013); <https://doi.org/10.1016/j.ceramint.2013.02.051>
- [27] S. Kang et al., *Nano Letters* 18, 467 (2018); <https://doi.org/10.1021/acs.nanolett.7b04416>
- [28] M. Chen et al., *Chemical Engineering Journal* 390, 124481 (2020); <https://doi.org/10.1016/j.cej.2020.124481>
- [29] J. Tian et al., *Journal of Oceanology and Limnology* 38, 1517 (2020); <https://doi.org/10.1007/s00343-020-9327-y>
- [30] M. Golestanbagh et al., *Catalysis Letters* 148(7), 2162 (2018); <https://doi.org/10.1007/s10562-018-2385-5>
- [31] H. Yamashita et al., *Applied Surface Science* 122, 305 (1997); [https://doi.org/10.1016/S0169-4332\(97\)00311-5](https://doi.org/10.1016/S0169-4332(97)00311-5)
- [32] R. Mohammadi et al., *Journal of Physical Chemistry A* 88(7), 1184 (2014); <https://doi.org/10.1134/S0036024414070243>
- [33] D. Y. C. Leung et al., *Chem Sus Chem* 3, 681 (2010).
- [34] M. Tang et al., *Material Research Express* 8, 085007 (2021); <https://doi.org/10.1088/2053-1591/ac1bcd>